ACS APPLIED MATERIALS & INTERFACES
Research Article
www.acsami.org

Surface Passivation of MoO_3 Nanorods by Atomic Layer Deposition toward High Rate Durable Li Ion Battery Anodes

B. Ahmed, Muhammad Shahid, D. H. Nagaraju, D. H. Anjum, Mohamed N. Hedhili, and H. N. Alshareef*

Materials Science and Engineering, King Abdullah University of Science and Technology (KAUST), Thuwal, 23955−6900, Saudi Arabia

Supporting Information

ABSTRACT: We demonstrate an effective strategy to overcome the degradation of MoO_3 nanorod anodes in lithium (Li) ion batteries at high-rate cycling. This is achieved by conformal nanoscale surface passivation of the MoO_3 nanorods by HfO_2 using atomic layer deposition (ALD). At high current density such as 1500 mA/g, the specific capacity of HfO_2-coated MoO_3 electrodes is 68% higher than that of bare MoO_3 electrodes after 50 charge/discharge cycles. After 50 charge/discharge cycles, HfO_2-coated MoO_3 electrodes exhibited specific capacity of 657 mAh/g; on the other hand, bare MoO_3 showed only 460 mAh/g. Furthermore, we observed that HfO_2-coated MoO_3 electrodes tend to stabilize faster than bare MoO_3 electrodes because nanoscale HfO_2 layer prevents structural degradation of MoO_3 nanorods. Additionally, the growth temperature of MoO_3 nanorods and the effect of HfO_2 layer thickness was studied and found to be important parameters for optimum battery performance. The growth temperature defines the microstructural features and HfO_2 layer thickness defines the diffusion coefficient of Li-ions through the passivation layer to the active material. Furthermore, ex situ high resolution transmission electron microscopy, X-ray photoelectron spectroscopy, Raman spectroscopy, and X-ray diffraction were carried out to explain the capacity retention mechanism after HfO_2 coating.

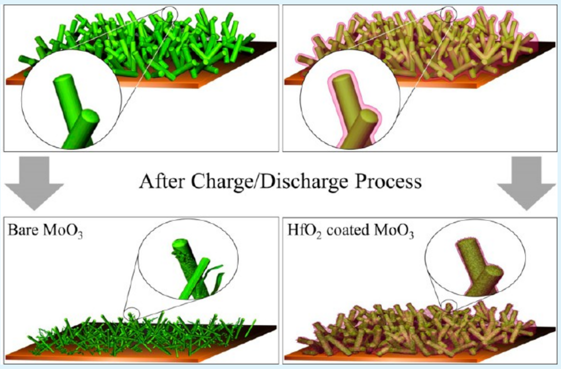

KEYWORDS: *MoO_3, atomic layer deposition (ALD), anode, lithium ion battery, TEM*

1. INTRODUCTION

Lithium ion batteries (LIBs) have been successfully commercialized in small power sources such as portable electronics and power tools because of their high energy density and stable cyclic performance.[1] Recently, LIBs are being extensively researched for large scale applications such as electric vehicles, hybrid vehicles, and power backups, which require both high energy and high power densities. However, lower specific power density (the ability to charge/discharge at very high rates) hinders their application in large scale energy storage. Therefore, a great deal of research effort has been focused on development of LIBs with high energy and high power densities.

Graphite is the most widely used anode material in commercially available LIBs but due to its low theoretical capacity (~372 mAh/g) it cannot meet the growing demand of high capacity energy storage system.[2] Thus, a lot of research effort has been made to discover new materials for Lithium (Li) storage with high capacity, rate capability, cycling stability, and safety to replace the widely used graphitic anode material.

One-dimensional (1D) nanostructures such as nanowires, nanobelts and nanorods showed great promise in energy storage applications due to large surface-to-volume ratio which increases the electrode−electrolyte contact area.[3,4] Furthermore, 1D materials act as efficient electron transport pathway and sustain volumetric expansion because of Li intercalation/deintercalation during charge/discharge process.[5,6] Consequently, 1D $LiMn_2O_4$,[5] V_2O_5,[6] TiO_2,[7] $Li_{0.88}[Li_{0.18}Co_{0.33}Mn_{0.49}]O_2$,[8] $Li_{0.44}MnO_2$,[9] Fe_3O_4,[10] and $Sn_{78}Ge_{22}$@carbon[11] nanowires have shown improved rate performances in energy storage devices. Recently, a vast amount of research focus has been devoted to 1D nanostructured transition metal oxides (TMOs) because of their unique morphology and high theoretical capacity.[12,13] Among them, molybdenum trioxide (MoO_3) is considered as an attractive anode material for LIBs because of its superior theoretical specific capacity (~1117 mAh/g).[14] MoO_3 was investigated during the early stage of lithium battery research as Li^+ insertion compound because of its stable layered structure which can host intercalated Li^+ ions.[15] In terms of crystal structure, MoO_3 exists in three different forms; orthorhombic (α-MoO_3), monoclinic (β-MoO_3), and hexagonal (h-MoO_3). Thermodynamically, α-MoO_3 is the most stable phase, and its anisotropic layered structure makes it a suitable candidate for LIBs.[15] The crystal structure of α-MoO_3 can be explained as double layers in the [010] direction, and each layer consists of two sublayers by sharing MoO_6 octahedrons along

Received: August 2, 2014
Accepted: June 3, 2015
Published: June 3, 2015

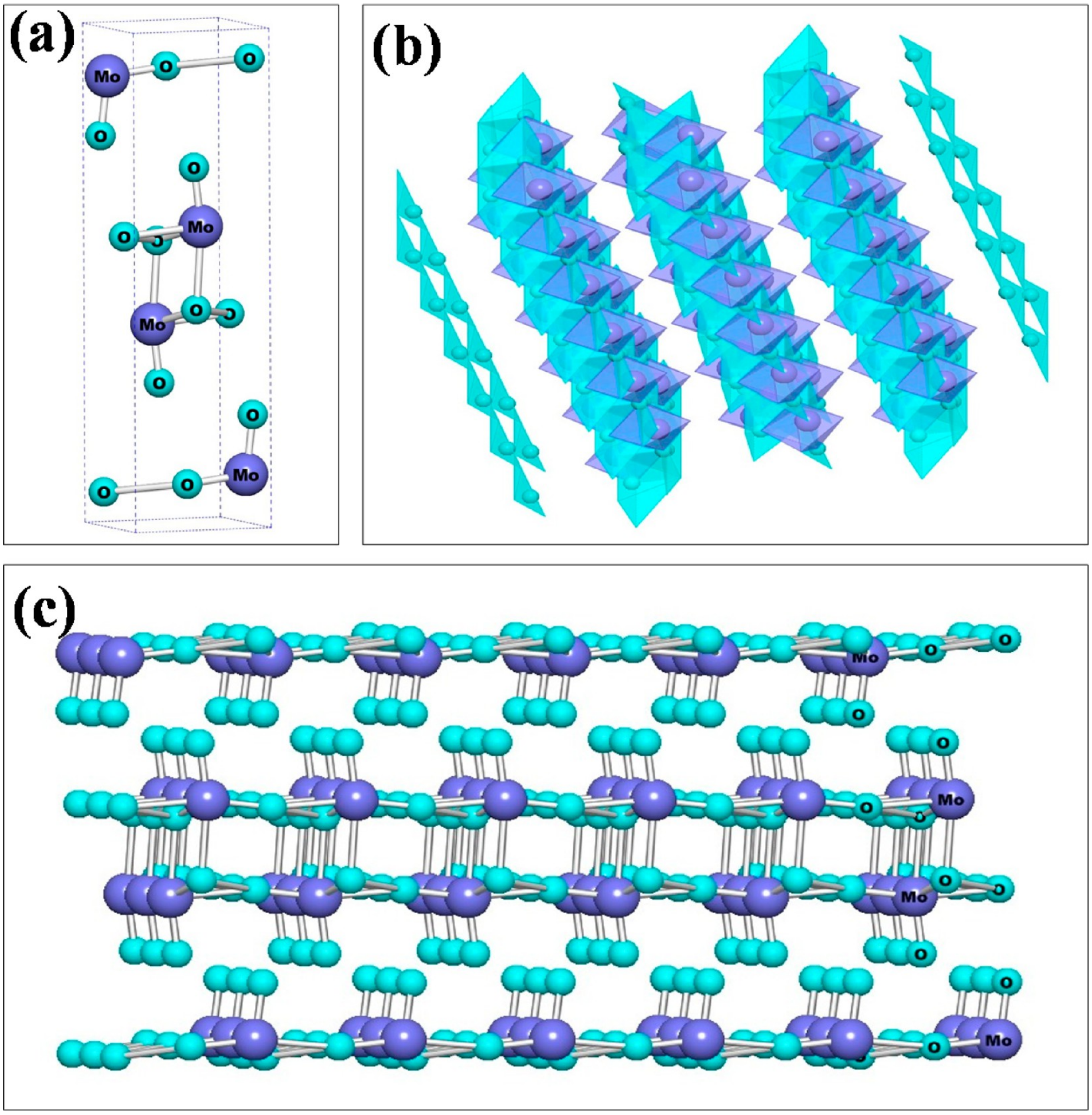

Figure 1. Schematic illustration of crystal structure of α-MoO_3: (a) unit cell and (b−c) showing layered nature of MoO_3.

the [100] and [001] directions.[16] The schematic illustration of unit cell and layered structure of α-MoO_3 is given in Figure 1. However, as an anode material in Li ion batteries, the poor conductivity and large volumetric changes during charge/discharge process limit the application of MoO_3 in LIBs.[17] It has been reported that volumetric expansion in metal oxides can be as high as 100−250% and due to this drastic volumetric change during intercalation/deintercalation of Li^+ ions, MoO_3 shows poor cyclic stability and capacity fades quickly.[18]

The cyclic stability and electrochemical performance of LIBs can be improved by a number of approaches. The most common approach is to optimize the nanostructure of active material such as conversion of bulk into nano sized powder, preparation of layered structure, or synthesis of 1D morphologies such as nanorods, nanowires, or nanobelts.[19,20] The deposition of a passivation layer at electrode/electrolyte interface to prevent structural degradation during charge/discharge process is another methodology.[21] Mostly, surface passivation layers are deposited by sol−gel method[22] or chemical vapor deposition technique;[23] however, these techniques lack control over thickness, surface coverage, and uniformity of coating. However, precise control over thickness is necessary to obtain optimum battery performance because Li^+ ions have to diffuse through the passivation layer and intercalate or react with active material. Moreover, these solution-based methods involve mixing electrode material with precursor followed by annealing at elevated temperature to form a coating layer. This post-annealing sometimes results in structural degradation of electrode material.

On the other hand, a thin and conformal layer with excellent control on growth rate can be deposited by atomic layer deposition (ALD) which uses sequential self−limiting gas/solid

DOI: 10.1021/acsami.5b03395
ACS Appl. Mater. Interfaces 2015, 7, 13154−13163

reactions.[24,25] The unique reaction mechanism of ALD offers exclusive advantages such as low temperature process, precise control over thickness and conformal coating even with high aspect ratio 3D structures.[25] In LIBs, ALD has been used to fabricate different electrode structures,[26−36] solid state electrolyte[37−41] and modify electrode/electrolyte interface.[18,42−56] ALD coating on electrode/electrolyte interface aims to avoid undesirable interfacial reactions which occur between the electrode and liquid electrolyte during charge/discharge process. These interfacial reactions compromise the overall performance of LIBs in terms of cyclic stability and safety. For instance, HF generated on the cathode side tends to consume the cathode material and results in poor cyclic performance.[57] On the anode side, ALD coatings mainly deal with the problems arising from the SEI such as decomposition products of liquid electrolytes.[58] These problems become more consequential in anodes where large volumetric changes occur during charge/discharge process such as tin oxide (SnO_2) and silicon (Si).

The ALD layer at anode/electrolyte interface serves as an artificial layer which hinders the formation of SEI layer and improves specific capacity, cyclic performance, and columbic efficiency.[42,43,50,51] Moreover, the problem of pulverization in different anode materials which goes under large volumetric changes during charge/discharge process such as Si,[45−49] SnO_2,[53] Fe_3O_4,[55] and ZnO[54] can be reduced by ALD surface coating. In published literature, ALD coating of Al_2O_3,[18,42,44−46,52,53,55,56] TiO_2,[43,48,49,54] ZrO_2,[51] TiN,[47,50] and HfO_2[59] on anode/electrolyte interface has been reported for different materials such as graphite,[42−44] patterned Si,[45] Si nanowires,[47] Si nanotubes,[49] Si films,[46] $Li_4Ti_5O_{12}$,[50−52] SnO_2,[53,59] ZnO,[54] and Fe_3O_4.[55] Besides coating material, growth temperature and layer thickness are the most important parameters in defining final device performance. Moreover, there are two approaches for ALD coating: coating on electrode material or coating on prepared electrode. It has been reported that the latter serves better in terms of battery performance and improvement in anode/electrolyte interface.[18] Furthermore, some reports focused to understand the mechanism of performance improvement due to ALD coating layer and various in situ or ex situ analysis techniques such as scanning ion conductance microscopy (SICM), electrical impedance spectroscopy (EIS) and transmission electron microscopy (TEM) have been utilized.[56] However, it is worth mentioning that the capacity retention mechanism varies from system to system, and therefore, it is of utmost importance to understand how different electrode materials and interfaces are modified by different ALD coating materials.

In this study, we deposited HfO_2 coating by ALD on 1D MoO_3 nanorods to enhance the electrochemical performance and overcome the poor cyclic stability. Two important parameters; the growth temperature of MoO_3 nanorods and HfO_2 thickness were optimized in terms of microstructure of MoO_3 and LIB performance. This study demonstrates remarkable performance improvement and cyclic stability of HfO_2-coated MoO_3 nanorods. Furthermore, we aim to understand the underlying capacity retention mechanism after HfO_2 coating by ex situ XRD, Raman spectroscopy, TEM, and XPS before and after charge/discharge process. Previously, we have reported the application of HfO_2 layer on SnO_2 nanospheres where cyclic stability of SnO_2 nanospheres has been improved after HfO_2 coating. This study shows that HfO_2 coating can be an effective way of improving cyclic stability in 1D nanostructured system, as well, and describes the capacity retention mechanism of HfO_2 coating.

2. EXPERIMENTAL SECTION

2.1. Synthesis of MoO_3 Nanorods and Characterization. MoO_3 nanorods were synthesized via one-step hydrothermal method. In a typical reaction, a certain amount of ammonium molybdate powder was dissolved in deionized water (DI) under continuous stirring to obtain a clear solution. The acidic pH of the solution was maintained by the addition of diluted hydrochloric acid (HCl) during stirring. After 2 h, the mixture was transferred to a Teflon lined stainless steel autoclave. The synthesis was carried out at the temperature range of 90−180 °C for 12 h. After the hydrothermal reaction, the autoclave was cooled to room temperature naturally, and a white precipitate was obtained. The resulting white precipitates of the MoO_3 nanorods were washed and filtered with DI water and ethanol and dried at 80 °C for 12 h in a vacuum oven.

Structural analysis of the samples was performed with the X-ray diffraction system (XRD, Bruker, D8 ADVANCE) using Cu Kα radiation of wavelength 1.5418 Å. Field emission scanning electron microscopy (FESEM, Nova Nano) and TEM (300 kV, FEI-CM30) were used to investigate the morphology of the MoO_3 nanorods and HfO_2-coated MoO_3 nanorods. Sample preparation for the TEM analysis was carried out by gently scraping the top layer of the HfO_2-coated MoO_3 electrode using a sharp stainless blade and collected powder was dispersed in ethanol by sonication for about 5 min. The dispersed solution was drop casted onto the TEM nickel grid and dried. Raman spectroscopic measurements were carried out using a LabRamAramis with a He−Ne laser having an excitation wavelength of 473 nm. XPS analysis was carried out in a Kratos Axis Ultra DLD spectrometer equipped with a monochromatic Al Kα X-ray source ($h\nu$ = 1486.6 eV) operating at 150 W, a multichannel plate and delay line detector under a vacuum of $\sim 10^{-9}$ mbar. The high-resolution spectra were collected at fixed analyzer pass energy of 20 eV. The binding energy was calibrated by taking the C 1s peak (284.4 eV) as a reference, which corresponds to acetylene black carbon before the electrochemical process. After the electrochemical process, the binding energy was calibrated by taking the C 1s peak (285.0 eV) as a reference corresponds to carbon, which is present on the electrode surface resulting from the decomposition of ethylene carbonate (EC) and dimethyl carbonate (DMC).

2.2. Electrode Fabrication, HfO_2 Coating and Electrochemical Characterization. The working electrodes were prepared by mixing the active material, MoO_3 nanorods, with methyl cellulose binder (Na-CMC, Sigma-Aldrich) and acetylene black (MTI, Inc.) as conductive additive in weight ratio of 70:15:15 in DI water to form a slurry. This slurry was uniformly pasted on a copper foil (MTI, Inc.) using a doctor blade and dried at 90 °C for 24 h in vacuum oven. Nanoscale HfO_2 layer was deposited on the prepared electrodes at 180 °C using atomic layer deposition system (Cambridge Nanotech Savannah). The HfO_2 ALD reaction sequence was (1) a constant N_2 dose at 20 psi; (2) H_2O dose for 0.015 s; (3) H_2O reaction time, 10 s; (4) Tetrakis (dimethylamino) hafnium ($Hf(NMe_2)_4$) dose to 0.2 s; and (5) $Hf(NMe_2)_4$ reaction time, 15 s. This sequence constitutes one ALD cycle of HfO_2. The growth rate per cycle is 0.10 nm per cycle at these conditions. The active material mass loading of the sample on the copper foil was maintained between 2.5 and 2.7 mg/cm^2.

Electrochemical measurements were carried out in 2032 coin cells (MTI, Inc.) using an electrochemical analyzer (VMP3, Biologic, Inc.). The lithium foil was used as the counter and a reference electrode. Celgard 2500 micro porous membranes were used as separators. The organic electrolyte was a mixture of lithium salt and organic solvents. Typically, $LiPF_6$ was dissolved in ethylene carbonate (EC)/dimethyl carbonate (DMC; 1:1 w/w) and a certain amount of electrolyte was used in each experiment. The cells were assembled in an argon-filled glovebox with the concentrations of moisture and oxygen below 0.1 ppm. The electrochemical performance of the devices was evaluated at various current densities ranging from 100 to 1500 mA/g between 0.01 to 3.00 V (vs Li/Li^+). Cyclic voltammetry was performed to examine the reduction and oxidation peaks between the voltage range of 3.0−0.005 V (vs Li/Li$^+$) at a scan rate of 0.2 mV/s. EIS was measured by applying a sine wave with an amplitude of 5.0 mV over the frequency range 1000 kHz to 0.01 Hz at open circuit voltage (OCV).

3. RESULTS AND DISCUSSIONS

3.1. Material Characterization. The hydrothermal reaction to prepare MoO_3 nanorods was carried out at four different temperatures, 90, 120, 150, and 180 °C, for 12 h. The morphology of final product was observed by field emission scanning electron microscope (FESEM). Figure 2 presents FESEM images of MoO_3 nanorods obtained at different growth temperatures. At 90 °C, rod-like structure was achieved with thickness of 700−800 nm but with increasing growth temperature, thicker nanorods gradually split into thinner nanorods. Finally, at 180 °C nanorods with uniform thickness of 100−250 nm and 5−10 μm length were formed. Figure 3 shows the TEM image of MoO_3 nanorods synthesized at 180 °C. The lattice spacing of 0.39 (Figure 3b) corresponds to (100) plane of orthorhombic α-MoO_3 structure.[16] The selected area electron diffraction pattern (SAED) recorded from the edge of α-MoO_3 nanorod is presented in inset of Figure 3a. The SAED pattern taken along ⟨010⟩ zone axis confirms that synthesized MoO_3 powder is single crystal in nature. Furthermore, crystallinity and phase formation was also confirmed by XRD and Raman spectroscopy. Figure 4 presents the XRD pattern of MoO_3 powders synthesized at different temperatures. In this XRD pattern, all diffraction peaks can be readily indexed to orthorhombic α-MoO_3 with JCPDS card number 89-7112. It is well-known that α-MoO_3 has a layered crystal structure that exhibits three strong intensity peaks for the (020), (040), and (060) diffraction planes with 2θ values of 12.3, 25.6, and 39°, respectively.[16] Similarly, the Raman spectroscopy results (Figure S1, SI) confirm that single-phase α-MoO_3 was formed when synthesis was carried out at 180 °C. The spectra display peaks at 159, 285, 334, 823, 667, and 996 cm^{-1}, all of which are characteristic Raman bands of MoO_3.

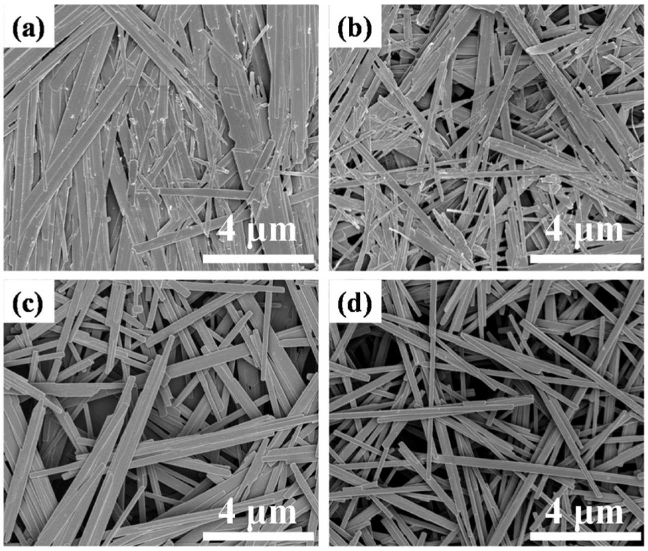

Figure 2. FESEM images of hydrothermally synthesized MoO_3 at (a) 90, (b) 120, (c) 150, and (d) 180 °C for 12 h.

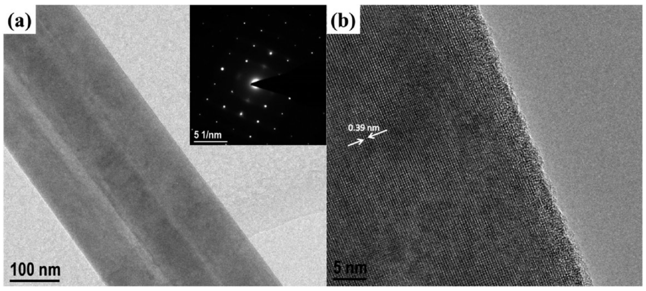

Figure 3. TEM images of MoO_3 nanorods synthesized at 180 °C: (a) low-magnification image of one MoO_3 nanorod, (inset) corresponding SAED pattern, and (b) high-resolution TEM image from a typical MoO_3 nanorod.

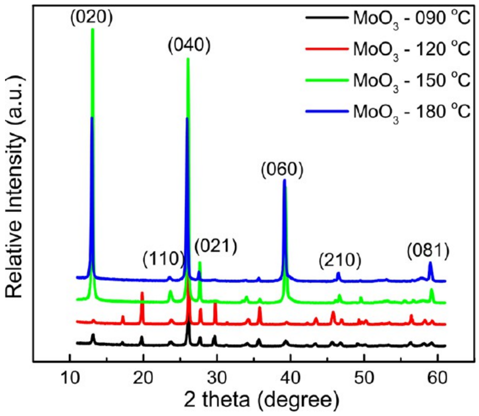

Figure 4. XRD patterns of hydrothermally synthesized MoO_3 at different temperatures for 12 h.

Finally, we carried out high-resolution transmission electron microscope (HRTEM) imaging of bare MoO_3 and HfO_2-coated MoO_3 nanorods to observe the uniformity and conformality of nanoscale HfO_2 layer. The HRTEM images of bare MoO_3 and HfO_2-coated MoO_3 are shown in Figure 5 for 0, 30, 50, and 80 ALD cycles. As mentioned earlier, the prime advantage of ALD is to deposit a thin layer with excellent thickness control; one can observe in HRTEM images that obtained thickness of HfO_2 layer is according to ALD processing conditions. It is worth noting that HRTEM images of HfO_2-coated MoO_3 nanorods in Figure 5b−d do not show lattice fringes, which confirms that HfO_2 layer is amorphous in nature. The deposition of HfO_2 on the surface of MoO_3 nanorods was confirmed by scanning transmission electron microscopy−energy dispersive spectroscopy (STEM−EDS). The composition of MoO_3 nanorods at the center and at the edge was examined by STEM−EDS and presented in Figure S2 (SI), which clearly indicates that HfO_2 is coated on the surface, and MoO_3 nanorods are completely covered by HfO_2 layer.

3.2. Electrochemical Characterization. The detailed electrochemical behavior of bare MoO_3 and HfO_2-coated MoO_3 (10 ALD cycles) electrodes was investigated by cyclic voltammetry (CV). Figure 6 shows the CV curves of bare MoO_3 and HfO_2-coated MoO_3 electrodes obtained at a scan rate of 0.2 mV/s in potential window of 0.005−3.0 V vs Li/Li$^+$. In Figure 6a, the first CV cycle of bare MoO_3 and HfO_2-coated MoO_3 electrodes is presented. The curves show typical peaks of MoO_3 in the oxidation and reduction reactions. In the first cycle, two peaks at around 2.2 and 2.6 V correspond to the intercalation/deintercalation of Li$^+$ ions into the interlayer

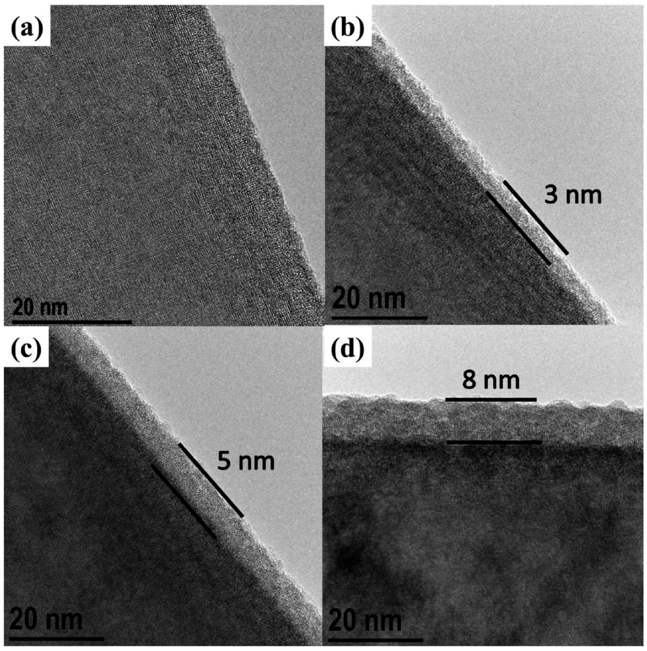

Figure 5. High-resolution TEM images of bare MoO_3 and HfO_2-coated MoO_3 powders: (a) 0, (b) 30, (c) 50, and (d) 80 ALD cycles.

spacing between the MoO_6 octahedron layers.[60] Figure 6b presents the second CV cycle of bare MoO_3 and HfO_2-coated MoO_3 electrodes, and it can be clearly observed that these peaks disappear in second cycle which can be because of loss of crystalline structure during the charge/discharge process.[60,61] Relatively weaker peaks at ∼1.6 V suggest the formation of MoO_2 phase, which indicates that the crystal structure of α-MoO_3 changes during charge/discharge process.[62] Furthermore, CV curves confirmed that HfO_2 does not take part in electrochemical reaction, as no additional peaks were observed for HfO_2-coated MoO_3 electrodes. This result is in good agreement with the previous report where HfO_2 was deposited on SnO_2 nanoparticles.[59]

Before moving further, we measured the cyclic performance of MoO_3 nanorods synthesized at different temperatures, and results are presented in Figure S3 (SI). The MoO_3 nanorods synthesized at 180 °C showed higher cyclic stability than the MoO_3 nanorods synthesized at 90, 120, and 150 °C. This is due to attainment of high crystallinity and morphology and this result is in good agreement with SEM, XRD, and Raman results discussed earlier. The similar effect of crystallinity on battery performance has been reported for other materials as well.[63,64] Afterward, MoO_3 nanorods synthesized at 180 °C were used for further electrochemical characterization. Furthermore, we have mentioned earlier that HfO_2 does not contribute to the device capacity and remain inactive during electrochemical process, but one should note that thickness of HfO_2 layer needs to be finely tuned for optimal battery performance. The thickness of the HfO_2 layer limits the rate of Li^+ ions diffusion through the ALD layer to active material. Therefore, we deposited different thicknesses of HfO_2 layer by varying the number of ALD cycles, and results are presented in Figure S4 (SI). We found that a 1 nm thick HfO_2 layer, which corresponds to 10 ALD cycles, performs better than thicker layers. One should note that a 1 nm layer of HfO_2 is an optimal compromise between Li^+ ion diffusion and passivation effects. Hence, cyclic performances of bare MoO_3 and HfO_2-coated MoO_3 electrodes were investigated with this optimized thickness of HfO_2 layer (∼1 nm).

Figure 7 shows the charge/discharge profiles for the 1st, 20th and 50th cycles at a current density of 100 mA/g between 0.01 and 3.0 V vs Li/Li^+ for bare MoO_3 and HfO_2-coated MoO_3 electrodes, respectively. The first discharge curve in both bare MoO_3 and HfO_2-coated MoO_3 electrodes showed three distinct voltage plateaus at 2.75, 2.35, and 0.40 V (vs Li^+/Li) which reconfirms that HfO_2 is electrochemically inactive. The voltage plateaus at 2.75 and 2.35 V (vs Li^+/Li) has already been reported[15] and corresponds to insertion of Li^+ ions in MoO_3 structure. Overall, lithium insertion in MoO_3 takes place in two steps, as given below:

$$V > 1.5: MoO_3 + xLi^+ + xe^- \rightarrow Li_xMoO_3 \tag{1}$$

$$V < 0.7: Li_xMoO_3 + yLi^+ + ye^- \rightarrow Mo + 3Li_2O \tag{2}$$

Generally, it is considered that reaction 1 provides reversible capacity, while reaction 2 is responsible for irreversible capacity losses because LiO_2 is primarily irreversible. However, presence of nanosize metallic particles in the system leads to the reversibility of LiO_2.[65,66] Previously, when bulk MoO_3 powder has been applied as anode material in Li ion batteries, only two voltage plateaus are observed (V > 1.5),[15] but the charge/discharge curves presented in Figure 7 show the largest Li^+ ion storage in the voltage <0.40 V. This effect comes from

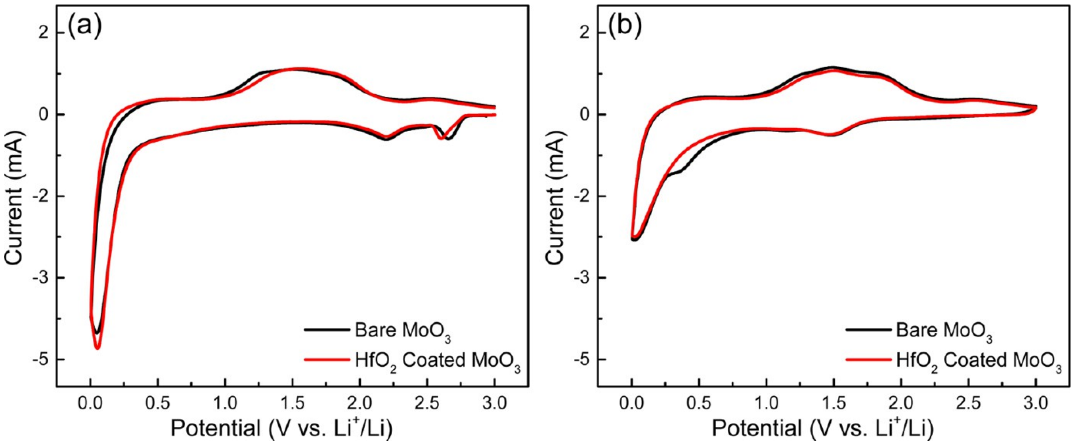

Figure 6. Cyclic voltammograms of bare MoO_3 and 10 ALD HfO_2-coated MoO_3 electrodes: (a) first cycle and (b) second cycle.

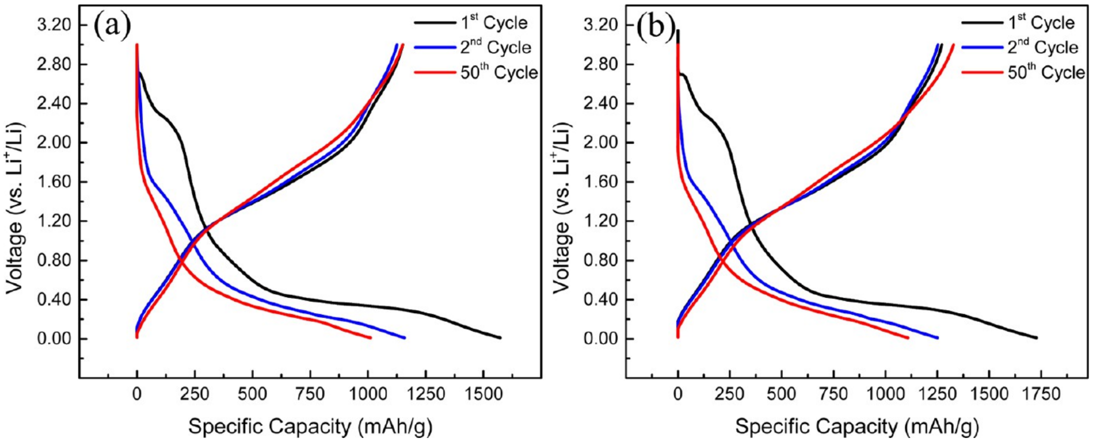

Figure 7. Charge/discharge curves measured at 100 mA/g: (a) bare MoO_3 and (b) 10 ALD HfO_2-coated MoO_3.

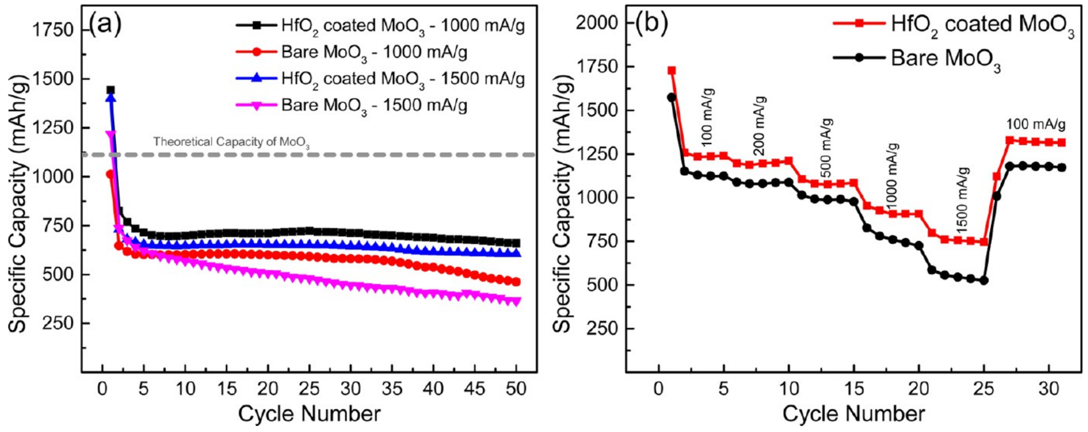

Figure 8. Electrochemical characterization: (a) cyclic performance at 1000 and 1500 mA/g and (b) rate−ability of bare MoO_3 and 10 ALD HfO_2-coated MoO_3 at different current densities.

nanostructure of MoO_3 nanorods and is mainly responsible for high specific capacity.[65] The first cycle discharge capacity was found to be 1573 and 1728 mAh/g for the bare MoO_3 and HfO_2-coated MoO_3 electrodes, respectively. Almost stable capacities of 1008 and 1120 mAh/g were obtained after 50 charge/discharge cycles for the bare MoO_3 and HfO_2-coated MoO_3 electrodes, respectively. The theoretical capacity of MoO_3 is about 1111 mAh/g;[14] however, the availability of large surface area and numerous reaction sites in nanostructured conversion reaction anodes provides higher capacity because they can afford additional surface dominated charge/discharge reactions with extra Li^+ ion adsorption/desorption.[67,68]

These results indicate that the HfO_2-coated MoO_3 nanorods have higher capacity and better electrochemical stability than bare MoO_3 electrodes. However, the effect of HfO_2 was not significant at low current density (100 mA/g). Therefore, bare MoO_3 and HfO_2-coated MoO_3 electrodes were studied at high current densities such as 1000 and 1500 mA/g. Figure 8a presents the cyclic performance of bare MoO_3 and HfO_2-coated MoO_3 electrodes measured at high current densities. Interestingly, the effect of HfO_2 layer on capacity retention is more significant at high current densities. For instance, at 1000 mA/g, after 50 charge/discharge cycles, the specific capacities of bare MoO_3 and HfO_2-coated MoO_3 electrodes are recorded as 460 mAh/g and 657 mAh/g, respectively. This is mainly because Li insertion/extraction during charge/discharge process involves large volumetric changes and the fast charge/discharge process would induce large stresses and accelerate capacity degradation.[18] The HfO_2 layer acts as a passivation layer; therefore, its effect is significant in fast charge/discharge processes. Additionally, we studied the rate capability of the bare MoO_3 and HfO_2-coated MoO_3 electrodes by subjecting electrodes under different current densities from 100 to 1500 mA/g, and results are presented in Figure 8b. At lower current densities (100, 200, and 500 mA/g), both bare MoO_3 and HfO_2-coated MoO_3 electrodes showed stable capacity, but at higher current densities (1000 and 1500 mA/g) the effect of HfO_2 became significant. At 1500 mA/g, the HfO_2 coated MoO_3 electrodes showed a specific capacity of 742 mAh/g, while bare MoO_3 showed 534 mAh/g. The results presented in Figure 8 clearly indicate that HfO_2 coating is an effective way of improving cyclic performance and high rate performance of MoO_3 nanorods. Previously, when ALD coated Al_2O_3 was applied on MoO_3 nanoparticles,[18] specific capacity of 900 mAh/g was observed after the 50th cycle. However, in this study, we observed higher capacity after the 50th cycle for HfO_2-coated MoO_3 electrode (~1120 mAh/g).

3.3. Ex Situ Electrode Analysis. Furthermore, the underlying capacity retention mechanism due to the HfO_2 coating was investigated by ex situ XRD, Raman spectroscopy, HRTEM, and XPS. The ex situ investigations were carried out on bare MoO_3 and HfO_2-coated MoO_3 electrodes before and after charge/discharge processes. Figure S5 (SI) shows the XRD spectra of bare MoO_3 and HfO_2-coated MoO_3 electrodes after 50 charge/discharge cycles. The XRD spectrum of MoO_3 nanorods before charge/discharge process displayed a layered crystalline structure (Figure 4), but the XRD spectrum of bare MoO_3 after 50 charge/discharge cycles lost the crystalline structure and does not show any characteristic diffraction peaks. The disappearance of high-intensity peaks at 12.3, 36.5, and 40.4° indicates that the MoO_3 structure becomes disordered during charge/discharge process, but it does not become completely amorphous. On the other hand, HfO_2-coated MoO_3 electrodes showed relatively more crystallinity after the charge/discharge process. Though all of the peaks cannot be indexed as single-phase α-MoO_3, crystallinity retention in HfO_2-coated MoO_3 electrodes is more than bare MoO_3 electrodes. The loss of crystallinity in bare MoO_3 electrodes after cycling has already been reported by other research groups, and they reported that it is the prime cause of capacity degradation in MoO_3 systems.[69] Similarly, the Raman spectra of as-prepared MoO_3 nanorods (Figure S1, SI) exhibited the characteristic Raman active bands of α-MoO_3 structure. However, after 50 charge/discharge cycles, α-MoO_3 peaks are lost in bare MoO_3 sample (Figure S6, SI). The ex situ XRD and Raman results suggested that HfO_2 coating somewhat slows the degradation of crystalline structure and acts as a barrier to the Li^+ ions during the charge/discharge process. Further confirmation of this observation was obtained by ex situ HRTEM measurements along with the selected area electron diffraction (SAED) patterns of bare MoO_3 and HfO_2-coated MoO_3 electrodes after 50 charge/discharge cycles. Figure 9 shows low- and high-magnification images and SAED patterns for bare MoO_3 and HfO_2-coated MoO_3 electrodes after 50 charge/discharge cycles. These results should be compared to Figure 3, in which HRTEM image and SAED pattern of as prepared MoO_3 nanorods are presented. It can be readily observed that highly crystalline structure of MoO_3 nanorods is severely degraded in the case of bare MoO_3 (Figure 9a−c), as evidenced by the disappearance of lattice fringes and distortion of SAED pattern. On the other hand, HfO_2-coated MoO_3 electrode showed that crystal structure of MoO_3 is also degraded to some extent but the degree of amorphousness is far less than bare MoO_3 electrode. This result is in good agreement with our observation in electrochemical data and ex situ XRD and Raman. On this basis, we conclude that nanoscale HfO_2 layer passivates anode/electrolyte interface and slows the structural degradation of electrode material. Moreover, amorphous nature of HfO_2 layer does not entirely block Li^+ ion diffusion and provides high rate performance.

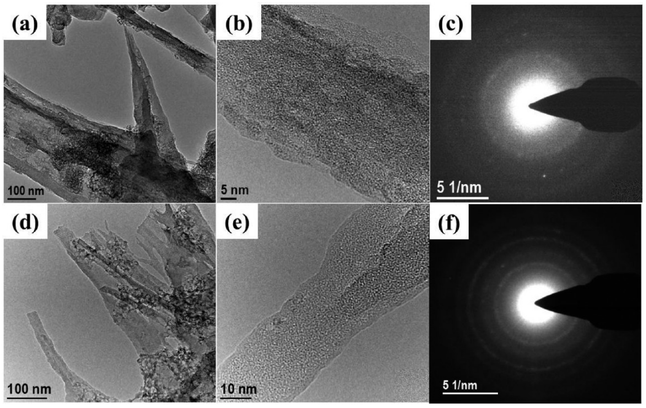

Figure 9. HRTEM analysis after 50 charge/discharge cycles: (a) low-magnification image, (b) high-magnification image, and (c) SAED pattern of bare MoO_3; and (d) low-magnification image, (e) high-magnification image, and (f) SAED pattern of HfO_2-coated MoO_3 electrodes.

Furthermore, ex situ XPS analysis was also performed on bare MoO_3 and HfO_2-coated MoO_3 electrodes before and after electrochemical process to determine the possible factors that lead to the observed difference in battery performance after HfO_2 coating. Figure S7 (SI) shows the typical XPS survey spectra of bare MoO_3 and HfO_2-coated MoO_3 electrodes before and after one charge/discharge cycle. Figure 10a,c shows high-resolution XPS spectra of the Hf 4f core level from electrodes coated with 1 nm HfO_2 layer, before and after one charge/discharge cycle. As shown in figure, the HfO_2-coated sample show $4f_{5/2}$ and $4f_{7/2}$ peaks from the HfO_2 indicating the presence of HfO_2 on the surface of MoO_3 nanorods. After one charge/discharge cycle, it was observed that the intensity of the HfO_2 peaks decreases sharply and their binding energy (B.E.) shifts. The B.E. of Hf $4f_{7/2}$ and $4f_{5/2}$ (in 1 nm HfO_2 layer) before electrochemical testing is at 17.31 and 18.98 eV, as shown in Figure 10a, and corresponds to HfO_2.[70] After one charge/discharge cycle, the B.E. of Hf $4f_{7/2}$ and Hf $4f_{5/2}$ decreased to 0.5 and 0.38 eV, respectively, as shown in Figure 10c. The shift in binding energy of HfO_2 is attributed to donation of charge from Hf to Mo which rises due to the difference in Pauling electronegativity between the Hf and Mo. This indicates that an efficient charge transfer process occurs during the electrochemical process for the HfO_2-coated MoO_3, which may help explain the improved behavior with HfO_2 coating.[59] The mechanism of charge transfer effect is unknown and requires more detailed in situ studies. In comparison, Figure 10b,d show the Mo 3d high-resolution XPS spectra for the HfO_2-coated MoO_3 nanorods before and after electrochemical process. The XPS spectra show the Mo $3d_{5/2}$ and Mo $3d_{3/2}$ peaks are located at 233 and 236 eV, as shown in Figure 10b. This binding energy corresponds to Mo in its highest oxidation state (i.e., Mo^{6+}), indicative of stoichiometric MoO_3 with traces of Mo^{5+} oxidation state at 231.56 eV. After one charge/discharge cycle, XPS spectrum shows no obvious shift in the binding energy of Mo $3d_{5/2}$ and Mo $3d_{3/2}$, as shown in Figure 10b,d. We also observed a peak at 230.4 eV, higher than the expected for Mo^{4+} (~229.5 eV) and lower than expected for Mo^{5+} (231.6). This could be attributed to $Mo^{+5-\delta}$ due to partial charge transfer from Li^+ to Mo_2O_5 after lithiation process. The appearance of Li 1s peak at B.E. of 55.2 eV after electrochemical process may be attributed to the presence of Li_2CO_3. The XPS results also confirmed that MoO_3 undergoes structural changes during charge/discharge process and HfO_2 assists the structural preservation.

In summary, we studied the electrochemical performance of bare MoO_3 and HfO_2-coated MoO_3 and demonstrated that 1 nm thin layer of HfO_2 deposited by ALD can significantly increase the cyclic performance of MoO_3 electrodes in Li ion batteries. Moreover, we explained the capacity retention mechanism and role of HfO_2 by ex situ analysis of electrodes before and after charge/discharge process. The proposed capacity retention mechanism has been summarized in Figure 11; bare MoO_3 nanorods structurally degrades after charge/discharge process and HfO_2-coated MoO_3 nanorods retain crystallinity and stability.

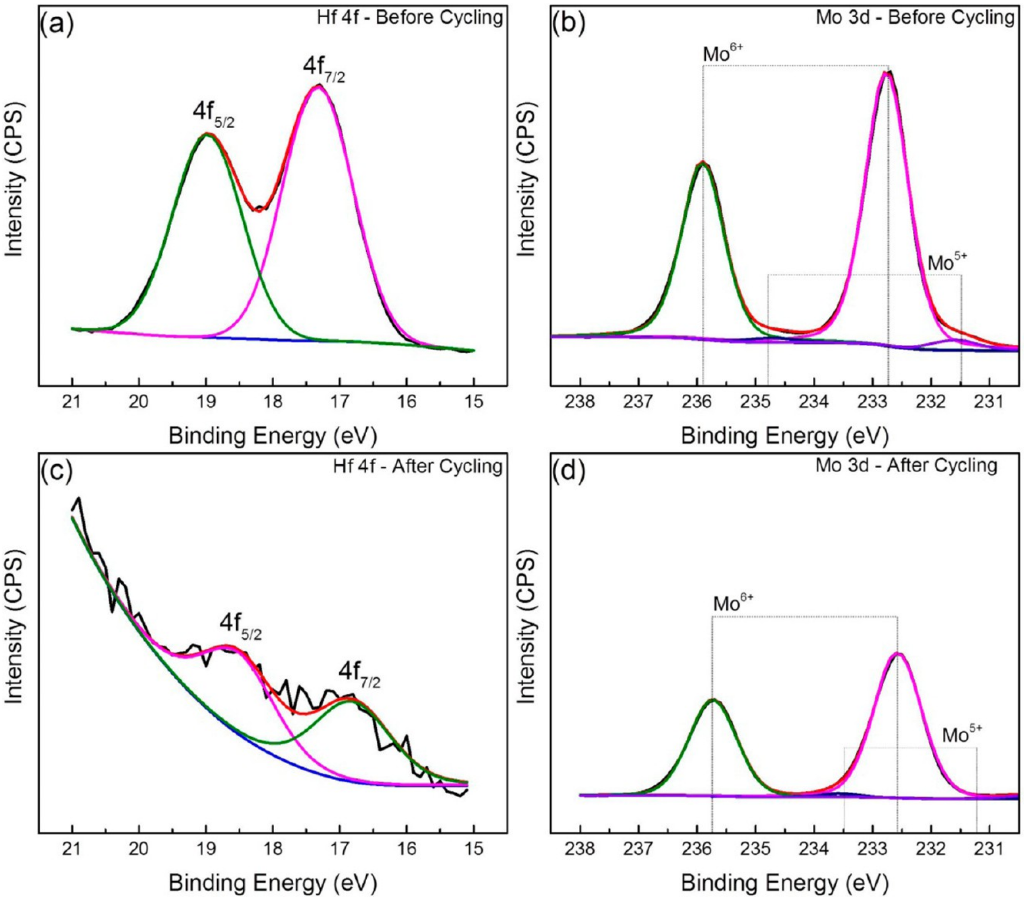

Figure 10. High-resolution XPS spectra of Hf 4f core level obtained from HfO_2-coated MoO_3 electrodes: (a) before and (c) after one charge/discharge cycle. Similar spectra for Mo 3d are shown (b) before and (d) after one charge/discharge cycle.

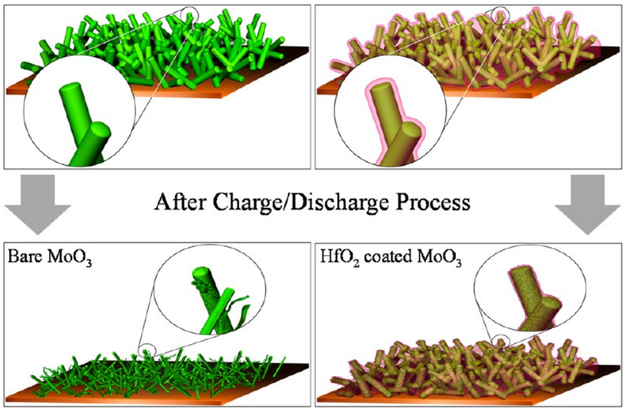

Figure 11. Schematic illustration of the proposed capacity retention mechanism: (left) bare MoO_3 and (right) HfO_2-coated MoO_3 electrodes before and after the charge/discharge process.

4. CONCLUSIONS

In conclusion, α-MoO_3 nanorods have been synthesized by hydrothermal method and applied as anode electrode in LIBs. The cyclic performance of MoO_3 nanorods has been improved by depositing a nanoscale HfO_2 layer using ALD. At high current density, the specific capacity of HfO_2-coated MoO_3 was found to be 68% higher than bare MoO_3 electrodes. Electrochemical measurements reveal that growth temperature of MoO_3 nanorods and optimization of the HfO_2 layer thickness needs to be finely tuned for optimal battery performance. It was observed that the effect of HfO_2 presence becomes more significant at high current densities such as 1000 and 1500 mA/g. This is mainly because charge/discharge process induces large volumetric changes, which results in internal stresses and passivation effect of HfO_2 is clearly observed in case of high rate cycling. Furthermore, the capacity retention mechanism was explained by ex situ HRTEM imaging and spectroscopy; XRD, Raman and XPS. The results showed that charge/discharge process distorts the crystal structure of MoO_3 and presence of HfO_2 layer serves as protective barrier at anode/electrolyte interface. Ex situ analysis clearly showed that HfO_2 assists in crystallinity retention and improves battery performance. These results indicate that HfO_2 coating can be an effective approach to improve cycling performance of MoO_3 anodes in LIBs.

■ ASSOCIATED CONTENT

Ⓢ Supporting Information

Raman spectra of MoO_3, STEM−EDS, effect of MoO_3 growth temperature on cyclic performance, effect of HfO_2 layer thickness on cyclic performance and ex situ XRD, Raman, and XPS results. The Supporting Information is available free of charge on the ACS Publications website at DOI: 10.1021/acsami.5b03395.

■ AUTHOR INFORMATION

Corresponding Author

*husam.alshareef@kaust.edu.sa.

Notes

The authors declare no competing financial interest.

ACKNOWLEDGMENTS

This research was supported by King Abdullah University of Science and Technology (KAUST).

REFERENCES

(1) Etacheri, V.; Marom, R.; Elazari, R.; Salitra, G.; Aurbach, D. Challenges in the Development of Advanced Li-Ion Batteries: A Review. *Energy Environ. Sci.* **2011**, *4*, 3243−3262.

(2) Tarascon, J. M.; Armand, M. Issues and Challenges Facing Rechargeable Lithium Batteries. *Nature* **2001**, *414*, 359−367.

(3) Guo, Y.-G.; Hu, J.-S.; Wan, L.-J. Nanostructured Materials for Electrochemical Energy Conversion and Storage Devices. *Adv. Mater.* **2008**, *20*, 2878−2887.

(4) Arico, A. S.; Bruce, P.; Scrosati, B.; Tarascon, J.-M.; van Schalkwijk, W. Nanostructured Materials for Advanced Energy Conversion and Storage Devices. *Nat. Mater.* **2005**, *4*, 366−377.

(5) Hosono, E.; Kudo, T.; Honma, I.; Matsuda, H.; Zhou, H. Synthesis of Single Crystalline Spinel $LiMn_2O_4$ Nanowires for a Lithium Ion Battery with High Power Density. *Nano Lett.* **2009**, *9*, 1045−1051.

(6) Chan, C. K.; Peng, H.; Twesten, R. D.; Jarausch, K.; Zhang, X. F.; Cui, Y. Fast, Completely Reversible Li Insertion in Vanadium Pentoxide Nanoribbons. *Nano Lett.* **2007**, *7*, 490−495.

(7) Armstrong, G.; Armstrong, A. R.; Bruce, P. G.; Reale, P.; Scrosati, B. TiO_2(B) Nanowires as an Improved Anode Material for Lithium-Ion Batteries Containing $LiFePO_4$ or $LiNi_{0.5}Mn_{1.5}O_4$ Cathodes and a Polymer Electrolyte. *Adv. Mater.* **2006**, *18*, 2597−2600.

(8) Lee, Y.; Kim, M. G.; Cho, J. Layered $Li_{0.88}[Li_{0.18}Co_{0.33}Mn_{0.49}]O_2$ Nanowires for Fast and High Capacity Li-Ion Storage Material. *Nano Lett.* **2008**, *8*, 957−961.

(9) Hosono, E.; Matsuda, H.; Saito, T.; Kudo, T.; Ichihara, M.; Honma, I.; Zhou, H. Synthesis of Single Crystalline $Li_{0.44}MnO_2$ Nanowires with Large Specific Capacity and Good High Current Density Property for a Positive Electrode of Li Ion Battery. *J. Power Sources* **2010**, *195*, 7098−7101.

(10) Taberna, P. L.; Mitra, S.; Poizot, P.; Simon, P.; Tarascon, J. M. High Rate Capabilities Fe_3O_4-Based Cu Nano-Architectured Electrodes for Lithium-Ion Battery Applications. *Nat. Mater.* **2006**, *5*, 567−573.

(11) Lee, H.; Cho, J. $Sn_{78}Ge_{22}$@Carbon Core−Shell Nanowires as Fast and High-Capacity Lithium Storage Media. *Nano Lett.* **2007**, *7*, 2638−2641.

(12) Poizot, P.; Laruelle, S.; Grugeon, S.; Dupont, L.; Tarascon, J. M. Nano-Sized Transition-Metal Oxides as Negative-Electrode Materials for Lithium-Ion Batteries. *Nature* **2000**, *407*, 496−499.

(13) Ku, J. H.; Jung, Y. S.; Lee, K. T.; Kim, C. H.; Oh, S. M. Thermoelectrochemically Activated MoO_2 Powder Electrode for Lithium Secondary Batteries. *J. Electrochem. Soc.* **2009**, *156*, A688−A693.

(14) Li, H.; Balaya, P.; Maier, J. Li-Storage via Heterogeneous Reaction in Selected Binary Metal Fluorides and Oxides. *J. Electrochem. Soc.* **2004**, *151*, A1878−A1885.

(15) Sasidharan, M.; Gunawardhana, N.; Noma, H.; Yoshio, M.; Nakashima, K. α-MoO_3 Hollow Nanospheres as an Anode Material for Li-Ion Batteries. *Bull. Chem. Soc. Jpn.* **2012**, *85*, 642−646.

(16) Zhou, L.; Yang, L.; Yuan, P.; Zou, J.; Wu, Y.; Yu, C. α-MoO_3 Nanobelts: A High-Performance Cathode Material for Lithium Ion Batteries. *J. Phys. Chem. C* **2010**, *114*, 21868−21872.

(17) Leroux, F.; Nazar, L. F. Uptake of Lithium by Layered Molybdenum Oxide and Its Tin Exchanged Derivatives: High Volumetric Capacity Materials. *Solid State Ionics* **2000**, *133*, 37−50.

(18) Riley, L. A.; Cavanagh, A. S.; George, S. M.; Jung, Y. S.; Yan, Y.; Lee, S.-H.; Dillon, A. C. Conformal Surface Coatings to Enable High Volume Expansion Li-Ion Anode Materials. *ChemPhysChem* **2010**, *11*, 2124−2130.

(19) Demir-Cakan, R.; Hu, Y. S.; Antonietti, M.; Maier, J.; Titirici, M. M. Facile One-Pot Synthesis of Mesoporous SnO_2 Microspheres via Nanoparticles Assembly and Lithium Storage Properties. *Chem. Mater.* **2008**, *20*, 1227−1229.

(20) Lou, X. W.; Wang, Y.; Yuan, C.; Lee, J. Y.; Archer, L. A. Template-Free Synthesis of SnO_2 Hollow Nanostructures with High Lithium Storage Capacity. *Adv. Mater.* **2006**, *18*, 2325−2329.

(21) Wang, L.; Wang, D.; Dong, Z.; Zhang, F.; Jin, J. Interface Chemistry Engineering for Stable Cycling of Reduced GO/SnO_2 Nanocomposites for Lithium Ion Battery. *Nano Lett.* **2013**, *13*, 1711−1716.

(22) Jeong, G.; Kim, J. H.; Kim, Y. U.; Kim, Y. J. Multifunctional TiO_2 Coating for a SiO Anode in Li-Ion Batteries. *J. Mater. Chem.* **2012**, *22*, 7999−8004.

(23) Xiao, J.; Xu, W.; Wang, D. Y.; Choi, D. W.; Wang, W.; Li, X. L.; Graff, G. L.; Liu, J.; Zhang, J. G. Stabilization of Silicon Anode for Li-Ion Batteries. *J. Electrochem. Soc.* **2010**, *157*, A1047−A1051.

(24) Miikkulainen, V.; Leskelä, M.; Ritala, M.; Puurunen, R. L. Crystallinity of Inorganic Films Grown by Atomic Layer Deposition: Overview and General Trends. *J. Appl. Phys.* **2013**, *113*, 021301.

(25) George, S. M. Atomic Layer Deposition: An Overview. *Chem. Rev.* **2010**, *110*, 111−131.

(26) Cheah, S. K.; Perre, E.; Rooth, M.; Fondell, M.; Hårsta, A.; Nyholm, L.; Boman, M.; Gustafsson, T.; Lu, J.; Simon, P.; Edström, K. Self-Supported Three-Dimensional Nanoelectrodes for Microbattery Applications. *Nano Lett.* **2009**, *9*, 3230−3233.

(27) Kim, S.-W.; Han, T. H.; Kim, J.; Gwon, H.; Moon, H.-S.; Kang, S.-W.; Kim, S. O.; Kang, K. Fabrication and Electrochemical Characterization of TiO_2 Three-Dimensional Nanonetwork Based on Peptide Assembly. *ACS Nano* **2009**, *3*, 1085−1090.

(28) Aravindan, V.; Jinesh, K. B.; Prabhakar, R. R.; Kale, V. S.; Madhavi, S. Atomic Layer Deposited (ALD) SnO_2 Anodes with Exceptional Cycleability for Li-Ion Batteries. *Nano Energy* **2013**, *2*, 720−725.

(29) Donders, M. E.; Knoops, H. C. M.; Kessels, W. M. M.; Notten, P. H. L. Co_3O_4 as Anode Material for Thin Film Micro-Batteries Prepared by Remote Plasma Atomic Layer Deposition. *J. Power Sources* **2012**, *203*, 72−77.

(30) Meng, X.; Libera, J. A.; Fister, T. T.; Zhou, H.; Hedlund, J. K.; Fenter, P.; Elam, J. W. Atomic Layer Deposition of Gallium Sulfide Films Using Hexakis(dimethylamido)digallium and Hydrogen Sulfide. *Chem. Mater.* **2014**, *26*, 1029−1039.

(31) Meng, X.; He, K.; Su, D.; Zhang, X.; Sun, C.; Ren, Y.; Wang, H.-H.; Weng, W.; Trahey, L.; Canlas, C. P.; Elam, J. W. Gallium Sulfide−Single-Walled Carbon Nanotube Composites: High-Performance Anodes for Lithium-Ion Batteries. *Adv. Funct. Mater.* **2014**, *24*, 5435−5442.

(32) Chen, X.; Zhu, H.; Chen, Y.-C.; Shang, Y.; Cao, A.; Hu, L.; Rubloff, G. W. MWCNT/V_2O_5 Core/Shell Sponge for High Areal Capacity and Power Density Li-Ion Cathodes. *ACS Nano* **2012**, *6*, 7948−7955.

(33) Chen, X.; Pomerantseva, E.; Banerjee, P.; Gregorczyk, K.; Ghodssi, R.; Rubloff, G. Ozone-Based Atomic Layer Deposition of Crystalline V_2O_5 Films for High Performance Electrochemical Energy Storage. *Chem. Mater.* **2012**, *24*, 1255−1261.

(34) Gandrud, K. B.; Pettersen, A.; Nilsen, O.; Fjellvag, H. High-Performing Iron Phosphate for Enhanced Lithium Ion Solid State Batteries as Grown by Atomic Layer Deposition. *J. Mater. Chem. A* **2013**, *1*, 9054−9059.

(35) Donders, M. E.; Arnoldbik, W. M.; Knoops, H. C. M.; Kessels, W. M. M.; Notten, P. H. L. Atomic Layer Deposition of $LiCoO_2$ Thin-Film Electrodes for All-Solid-State Li-Ion Micro-Batteries. *J. Electrochem. Soc.* **2013**, *160*, A3066−A3071.

(36) Liu, J.; Banis, M. N.; Sun, Q.; Lushington, A.; Li, R.; Sham, T.-K.; Sun, X. Rational Design of Atomic-Layer-Deposited $LiFePO_4$ as a High-Performance Cathode for Lithium-Ion Batteries. *Adv. Mater.* **2014**, *26*, 6472−6477.

(37) Aaltonen, T.; Nilsen, O.; Magrasó, A.; Fjellvåg, H. Atomic Layer Deposition of $Li_2O-Al_2O_3$ Thin Films. *Chem. Mater.* **2011**, *23*, 4669−4675.

(38) Comstock, D. J.; Elam, J. W. Mechanistic Study of Lithium Aluminum Oxide Atomic Layer Deposition. *J. Phys. Chem. C* **2013**, *117*, 1677−1683.

(39) Liu, J.; Banis, M. N.; Li, X.; Lushington, A.; Cai, M.; Li, R.; Sham, T.-K.; Sun, X. Atomic Layer Deposition of Lithium Tantalate Solid-State Electrolytes. *J. Phys. Chem. C* **2013**, *117*, 20260−20267.

(40) Ostreng, E.; Sonsteby, H. H.; Sajavaara, T.; Nilsen, O.; Fjellvag, H. Atomic Layer Deposition of Ferroelectric $LiNbO_3$. *J. Mater. Chem. C* **2013**, *1*, 4283−4290.

(41) Perng, Y.-C.; Cho, J.; Sun, S. Y.; Membreno, D.; Cirigliano, N.; Dunn, B.; Chang, J. P. Synthesis of Ion Conducting Lixalysizo Thin Films by Atomic Layer Deposition. *J. Mater. Chem. A* **2014**, *2*, 9566−9573.

(42) Jung, Y. S.; Cavanagh, A. S.; Riley, L. A.; Kang, S.-H.; Dillon, A. C.; Groner, M. D.; George, S. M.; Lee, S.-H. Ultrathin Direct Atomic Layer Deposition on Composite Electrodes for Highly Durable and Safe Li-Ion Batteries. *Adv. Mater.* **2010**, *22*, 2172−2176.

(43) Lee, M.-L.; Su, C.-Y.; Lin, Y.-H.; Liao, S.-C.; Chen, J.-M.; Perng, T.-P.; Yeh, J.-W.; Shih, H. C. Atomic Layer Deposition of TiO_2 on Negative Electrode for Lithium Ion Batteries. *J. Power Sources* **2013**, *244*, 410−416.

(44) Wang, H.-Y.; Wang, F.-M. Electrochemical Investigation of an Artificial Solid Electrolyte Interface for Improving the Cycle-Ability of Lithium Ion Batteries Using an Atomic Layer Deposition on a Graphite Electrode. *J. Power Sources* **2013**, *233*, 1−5.

(45) He, Y.; Yu, X.; Wang, Y.; Li, H.; Huang, X. Alumina-Coated Patterned Amorphous Silicon as the Anode for a Lithium-Ion Battery with High Coulombic Efficiency. *Adv. Mater.* **2011**, *23*, 4938−4941.

(46) Xiao, X.; Lu, P.; Ahn, D. Ultrathin Multifunctional Oxide Coatings for Lithium Ion Batteries. *Adv. Mater.* **2011**, *23*, 3911−3915.

(47) Kohandehghan, A.; Kalisvaart, P.; Cui, K.; Kupsta, M.; Memarzadeh, E.; Mitlin, D. Silicon Nanowire Lithium-Ion Battery Anodes with ALD Deposited Tin Coatings Demonstrate a Major Improvement in Cycling Performance. *J. Mater. Chem. A* **2013**, *1*, 12850−12861.

(48) Memarzadeh Lotfabad, E.; Kalisvaart, P.; Cui, K.; Kohandehghan, A.; Kupsta, M.; Olsen, B.; Mitlin, D. ALD TiO_2 Coated Silicon Nanowires for Lithium Ion Battery Anodes with Enhanced Cycling Stability and Coulombic Efficiency. *Phys. Chem. Chem. Phys.* **2013**, *15*, 13646−13657.

(49) Lotfabad, E. M.; Kalisvaart, P.; Kohandehghan, A.; Cui, K.; Kupsta, M.; Farbod, B.; Mitlin, D. Si Nanotubes ALD Coated with TiO_2, Tin or Al_2O_3 as High Performance Lithium Ion Battery Anodes. *J. Mater. Chem. A* **2014**, *2*, 2504−2516.

(50) Snyder, M. Q.; Trebukhova, S. A.; Ravdel, B.; Wheeler, M. C.; DiCarlo, J.; Tripp, C. P.; DeSisto, W. J. Synthesis and Characterization of Atomic Layer Deposited Titanium Nitride Thin Films on Lithium Titanate Spinel Powder as a Lithium-Ion Battery Anode. *J. Power Sources* **2007**, *165*, 379−385.

(51) Liu, J.; Li, X.; Cai, M.; Li, R.; Sun, X. Ultrathin Atomic Layer Deposited ZrO_2 Coating to Enhance the Electrochemical Performance of $Li_4Ti_5O_{12}$ as an Anode Material. *Electrochim. Acta* **2013**, *93*, 195−201.

(52) Ahn, D.; Xiao, X. Extended Lithium Titanate Cycling Potential Window with near Zero Capacity Loss. *Electrochem. Commun.* **2011**, *13*, 796−799.

(53) Wang, D.; Yang, J.; Liu, J.; Li, X.; Li, R.; Cai, M.; Sham, T.-K.; Sun, X. Atomic Layer Deposited Coatings to Significantly Stabilize Anodes for Li Ion Batteries: Effects of Coating Thickness and the Size of Anode Particles. *J. Mater. Chem. A* **2014**, *2*, 2306−2312.

(54) Lee, J.-H.; Hon, M.-H.; Chung, Y.-W.; Leu, I.-C. The Effect of TiO_2 Coating on the Electrochemical Performance of ZnO Nanorod as the Anode Material for Lithium-Ion Battery. *Appl. Phys. A: Mater. Sci. Process.* **2011**, *102*, 545−550.

(55) Kang, E.; Jung, Y. S.; Cavanagh, A. S.; Kim, G.-H.; George, S. M.; Dillon, A. C.; Kim, J. K.; Lee, J. Fe_3O_4 Nanoparticles Confined in Mesocellular Carbon Foam for High Performance Anode Materials for Lithium-Ion Batteries. *Adv. Funct. Mater.* **2011**, *21*, 2430−2438.

(56) Lipson, A. L.; Puntambekar, K.; Comstock, D. J.; Meng, X.; Geier, M. L.; Elam, J. W.; Hersam, M. C. Nanoscale Investigation of Solid Electrolyte Interphase Inhibition on Li-Ion Battery MnO Electrodes via Atomic Layer Deposition of Al_2O_3. *Chem. Mater.* **2014**, *26*, 935−940.

(57) Li, C.; Zhang, H. P.; Fu, L. J.; Liu, H.; Wu, Y. P.; Rahm, E.; Holze, R.; Wu, H. Q. Cathode Materials Modified by Surface Coating for Lithium Ion Batteries. *Electrochim. Acta* **2006**, *51*, 3872−3883.

(58) Jian, L.; Xueliang, S. Elegant Design of Electrode and Electrode/Electrolyte Interface in Lithium-Ion Batteries by Atomic Layer Deposition. *Nanotechnology* **2015**, *26*, 024001.

(59) Yesibolati, N.; Shahid, M.; Chen, W.; Hedhili, M. N.; Reuter, M. C.; Ross, F. M.; Alshareef, H. N. SnO_2 Anode Surface Passivation by Atomic Layer Deposited HfO_2 Improves Li-Ion Battery Performance. *Small* **2014**, *10*, 2849−2858.

(60) Li, W.; Cheng, F.; Tao, Z.; Chen, J. Vapor-Transportation Preparation and Reversible Lithium Intercalation/Deintercalation of α-MoO_3 Microrods. *J. Phys. Chem. B* **2006**, *110*, 119−124.

(61) Chen, J. S.; Cheah, Y. L.; Madhavi, S.; Lou, X. W. Fast Synthesis of α-MoO_3 Nanorods with Controlled Aspect Ratios and their Enhanced Lithium Storage Capabilities. *J. Phys. Chem. C* **2010**, *114*, 8675−8678.

(62) Sun, Y.; Wang, J.; Zhao, B.; Cai, R.; Ran, R.; Shao, Z. Binder-Free α-MoO_3 Nanobelt Electrode for Lithium-Ion Batteries Utilizing van der Waals Forces for Film Formation and Connection with Current Collector. *J. Mater. Chem. A* **2013**, *1*, 4736−4746.

(63) Wang, L.; Yu, Y.; Chen, P. C.; Zhang, D. W.; Chen, C. H. Electrospinning Synthesis of C/Fe_3O_4 Composite Nanofibers and their Application for High Performance Lithium-Ion Batteries. *J. Power Sources* **2008**, *183*, 717−723.

(64) Jung, Y. S.; Lee, S.; Ahn, D.; Dillon, A. C.; Lee, S.-H. Electrochemical Reactivity of Ball-Milled MoO_{3-y} as Anode Materials for Lithium-Ion Batteries. *J. Power Sources* **2009**, *188*, 286−291.

(65) Meduri, P.; Clark, E.; Kim, J. H.; Dayalan, E.; Sumanasekera, G. U.; Sunkara, M. K. MoO_{3-x} Nanowire Arrays as Stable and High-Capacity Anodes for Lithium Ion Batteries. *Nano Lett.* **2012**, *12*, 1784−1788.

(66) Meduri, P.; Pendyala, C.; Kumar, V.; Sumanasekera, G. U.; Sunkara, M. K. Hybrid Tin Oxide Nanowires as Stable and High Capacity Anodes for Li-Ion Batteries. *Nano Lett.* **2009**, *9*, 612−616.

(67) Dylla, A. G.; Xiao, P.; Henkelman, G.; Stevenson, K. J. Morphological Dependence of Lithium Insertion in Nanocrystalline $TiO_{2(\beta)}$ Nanoparticles and Nanosheets. *J. Phys. Chem. Lett.* **2012**, *3*, 2015−2019.

(68) Hu, Y.-Y.; Liu, Z.; Nam, K.-W.; Borkiewicz, O. J.; Cheng, J.; Hua, X.; Dunstan, M. T.; Yu, X.; Wiaderek, K. M.; Du, L.-S.; Chapman, K. W.; Chupas, P. J.; Yang, X.-Q.; Grey, C. P. Origin of Additional Capacities in Metal Oxide Lithium-Ion Battery Electrodes. *Nat. Mater.* **2013**, *12*, 1130−1136.

(69) Lee, S.-H.; Kim, Y.-H.; Deshpande, R.; Parilla, P. A.; Whitney, E.; Gillaspie, D. T.; Jones, K. M.; Mahan, A. H.; Zhang, S.; Dillon, A. C. Reversible Lithium-Ion Insertion in Molybdenum Oxide Nanoparticles. *Adv. Mater.* **2008**, *20*, 3627−3632.

(70) Renault, O.; Samour, D.; Rouchon, D.; Holliger, P.; Papon, A. M.; Blin, D.; Marthon, S. Interface Properties of Ultra-Thin HfO_2 Films Grown by Atomic Layer Deposition on SiO_2/Si. *Thin Solid Films* **2003**, *428*, 190−194.